MALAYSIAN JOURNAL OF MICROSCOPY

Journal homepage: https://malaysianjournalofmicroscopy.org

RESEARCH ARTICLE

OPTIMIZATION OF ANNEALING DURATION FOR ENHANCED MICROSTRUCTURE AND PROPERTIES IN A Zn-2.4Mn ALLOY

Kar Fei Chan[1], Ng Cong Li[1], Batrisyia Balqis[1], Yazid Yaakob[2], Hidetoshi Miyazaki[3], Masaki Tanemura[3], Mohd Zamri Mohd Yusop[1,*]

[1]Department of Materials, Manufacturing and Industrial Engineering, Faculty of Mechanical Engineering, Universiti Teknologi Malaysia, 81310 Johor Bahru, Johor, Malaysia.
[2]Department of Physics, Faculty of Science, Universiti Putra Malaysia, 43400 Serdang, Selangor, Malaysia.
[3]Department of Physical Science and Engineering, Nagoya Institute of Technology, 466-8555 Nagoya, Aichi, Japan.

Abstract. This study investigates the microstructural evolution and mechanical response of a Zn-2.4Mn alloy subjected to controlled heat treatments. The alloy was evaluated in as-cast, homogenised (390 °C), and annealed states (400 °C for 1-4 h) using optical microscopy, grain segmentation, Vickers hardness, tensile testing, and indentation cross-section analysis. The as-cast Zn-2.4Mn exhibited coarse dendritic grains with significant Mn segregation (grain area 5416.55 μm²) and poor mechanical properties: UTS of 28.33 MPa and elongation of 2.84 %. Homogenisation reduced chemical gradients but increased measured grain area to 6834.19 μm² due to dissolution of fine dendritic boundaries, while UTS improved to 102.06 MPa and elongation to 6.10 %. Recrystallisation initiated after 1 h of annealing (grain area 4684.46 μm²; UTS 103.38 MPa; elongation 4.38 %) and progressed to full refinement by 3 h, producing the minimum grain area of 3263.32 μm². Hardness increased from 53.12 HV (as-cast) to 73.13 HV at 3 h, while tensile performance reached its optimum (UTS 152.92 MPa, elongation 7.31 %). Indentation analysis confirmed the 3 h condition produced the most uniform deformation profile. Prolonged annealing to 4 h resulted in grain coarsening (4168.23 μm²), decreasing UTS to 113.25 MPa and elongation to 4.59 %, while hardness increased slightly to 74.73 HV, suggesting supplementary strengthening from residual $MnZn_{13}$ precipitates. These results demonstrate that annealing at 400 °C for 3 h provides the optimal balance of grain refinement, strength, and ductility for the Zn-2.4Mn alloy, establishing a clear processing–microstructure–property relationship.

Keywords: Zn-Mn alloy, plastic deformation, Vickers hardness, heat-treatment process, metallurgy.

Article Info

Received 9 January 2026
Accepted 6 May 2026
Published 8 June 2026

***Corresponding author: zamriyusop@utm.my**

ISSN: 1823-7010, eISSN: 2600-7444

1. INTRODUCTION

Zinc and its alloys have gained considerable attention as candidates for next-generation biodegradable implants, particularly in orthopedic applications, due to their moderate corrosion rate, favorable biocompatibility, and degradation kinetics that align more closely with bone healing compared to magnesium or iron-based systems [1-4]. Magnesium alloys tend to degrade too rapidly, compromising mechanical integrity, whereas iron-based systems degrade too slowly, delaying resorption and tissue regeneration [5-7]. Alloying zinc with elements such as Li, Mg, Ca, Sr, Mn, and Ag has been shown to markedly enhance mechanical properties approaching or surpassing the requirements for load-bearing applications while also improving cytocompatibility, osteogenic activity, and antibacterial behaviour [8, 9]. Although pure zinc suffers from limited strength and ductility [10, 11], recent advances in alloy design, thermomechanical processing, and microstructural tailoring have positioned zinc-based alloys as compelling alternatives for bioresorbable implant technologies [12-14].

Among these systems, Zn–Mn alloys have emerged as particularly promising due to the strong solid-solution and precipitation-based strengthening effects introduced by manganese, which significantly improves yield strength, ultimate tensile strength, and ductility while maintaining acceptable degradation rates in physiological environments [15]. Reported mechanical performance includes tensile strengths exceeding 110 MPa with elongation values above 10 %, alongside enhanced hardness and improved resistance to localized corrosion all critical parameters for maintaining temporary structural support during bone healing [16]. Manganese additions also promote favorable cellular responses, with in vitro studies demonstrating high cell viability and evidence of enhanced osteogenic differentiation, supporting their suitability for orthopedic fixation and bone-interfacing devices [17]. Furthermore, Zn–Mn alloys exhibit improved stability against pitting corrosion and support more uniform degradation compared to pure zinc, contributing to more predictable resorption behaviour in vivo [18].

Despite these advantages, challenges remain in optimizing the microstructure–property relationships of Zn–Mn alloys, particularly with respect to controlling corrosion rate, ensuring mechanical stability throughout the degradation process, and minimizing variability introduced by processing conditions. The formation of intermetallic phases such as $MnZn_{13}$ can improve strength and corrosion resistance, but their morphology, distribution, and thermal stability are highly sensitive to heat-treatment parameters [19]. Thermomechanical routes including homogenization, annealing, and high-pressure processing strongly influence grain size, defect density, and phase distribution, ultimately governing the mechanical and corrosion performance of the alloy [20]. Achieving a balance between mechanical reliability, predictable degradation kinetics, and favorable biological interactions requires a systematic understanding of how processing steps modify the microstructure of alloy and deformation behaviour [21].

In this study, a binary Zn-2.4Mn alloy was fabricated via melt casting, followed by homogenization and controlled annealing treatments at 390 °C for durations of 1, 2, 3, and 4 h [11, 22, 23]. The objective is to elucidate the influence of annealing duration on microstructural evolution and mechanical behaviour, with emphasis on grain growth, hardness variation, and localized deformation under indentation. Optical microscopy was used to assess surface morphology and grain structure, while Vickers micro-indentation provided insight into hardness and indentation topography, including pile-up and sink-in characteristics. Tensile testing was also performed to evaluate the macroscopic mechanical response across all processing conditions. Through this integrated analysis, the study aims to establish processing guidelines that optimize the microstructure of Zn-2.4Mn alloys for enhanced performance in biodegradable implant applications.

2. MATERIALS AND METHODS

High-purity zinc granules (99.72 %, C1109, HmbG Chemicals) and manganese metal powder (99.2 %, C1971, Bendosen) were used as received. A total mass of 2000 g was prepared by weighing

zinc (97.6 wt.%) and manganese (2.4 wt.%), followed by mixing in ethanol to ensure uniform dispersion. The mixture was transferred into a graphite crucible and melted in an electric resistance furnace preheated to 850 °C. After one hour of holding at this temperature, the molten alloy was poured into a preheated graphite mould heated separately using a torch to minimize thermal shock. The cast ingot was allowed to air-cool to room temperature overnight. Post-casting, the alloy ingot underwent homogenization at 390 °C for 3 hours, followed by furnace cooling. Subsequent annealing treatments were applied at 400 °C for durations of 1, 2, 3, and 4 h, each followed by furnace cooling. Control samples corresponding to the as cast and homogenised conditions were also retained. The overall processing sequence is schematically illustrated in Figure 1.

The heat-treated alloy was then machined using CNC milling (Millstar VH550 Series Vertical Milling Machine) into plates of 10 mm × 10 mm × 3 mm (six specimens per condition) and tensile specimens conforming to ASTM E8 geometry (thirty specimens in total). Prior to microstructural and surface assessments, the 10 mm × 10 mm × 3 mm samples were ground using SiC papers from P1000 to P3000 and subsequently polished with an Al_2O_3 suspension to achieve a mirror-finished surface suitable for indentation and optical examination.

Mechanical testing comprised Vickers microhardness measurements and uniaxial tensile testing. Vickers hardness was evaluated using a Matsuzawa DVK-2 microhardness tester with an applied load of 49 N, a loading rate of 100 µm/s, and a dwell time of 15 s. For each condition, multiple indentations were performed to ensure statistical reliability. Tensile testing of ASTM E8 specimens was conducted using a Shimadzu AGS-20kNx universal testing machine operating at room temperature with a constant crosshead speed of 1 mm/min. Five repetitions per processing condition were performed to determine ultimate tensile strength (UTS), yield strength, and elongation at fracture.

Surface topography around Vickers indentations and fracture morphologies from tensile specimens were examined using a Keyence VHX-7000N optical microscope. Images were captured at magnifications ranging from 20× to 200× to resolve both global surface features and localized deformation characteristics.

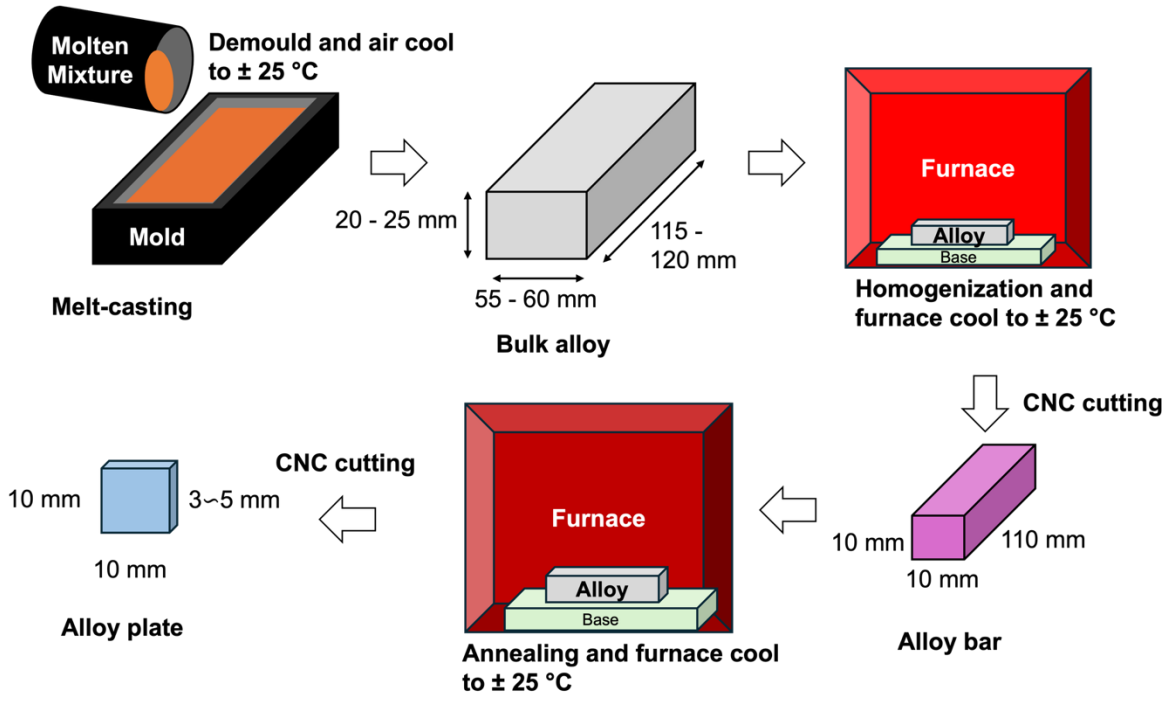

Figure 1: Experimental process including melt-casting, homogenization, annealing and cutting of Zn-2.4Mn alloy

3. RESULTS AND DISCUSSION

3.1 Microstructural Evolution During Heat Treatment

The optical micrographs and segmentation maps presented in Figures 2 and 3 reveal the systematic evolution of the Zn-2.4Mn alloy microstructure across the six thermal processing conditions. Each stage reflects the progressive transformation from a cast dendritic network into a recrystallised structure and, ultimately, a coarsened grain morphology at extended annealing durations.

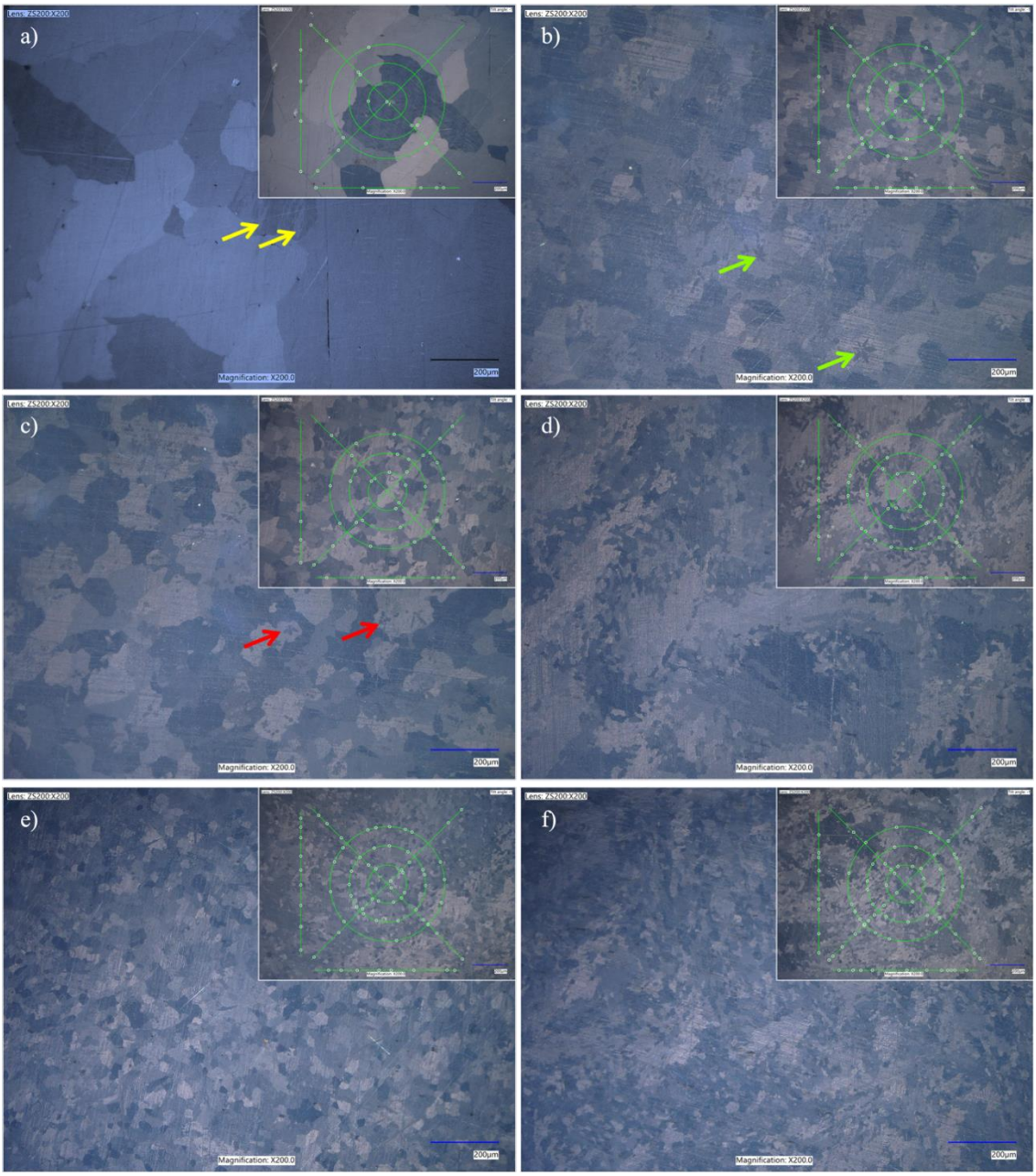

Figure 2: Optical micrographs of the Zn-2.4Mn alloy showing the evolution of interdendritic morphology across processing conditions: (a) as-cast, (b) homogenised, (c) annealed 1 h, (d) annealed 2 h, (e) annealed 3 h, and (f) annealed 4 h. Arrows highlight dendritic formation, dissolution, and retained interdendritic regions where relevant. Inset shows the grain segmentation point for each sample

The as-cast microstructure (Figure 2(a)) is dominated by coarse dendrites and clearly visible interdendritic regions (yellow arrows), typical of non-equilibrium solidification in Zn-Mn systems. The dendritic arms form large, irregular grains, reflected in the segmentation map (Figure 3(a)) where only a few oversized grains occupy the scanned area. Grain boundaries are diffuse and poorly defined, indicating a microstructure with high residual strain energy and solute segregation. These features establish the structural baseline prior to thermal refinement.

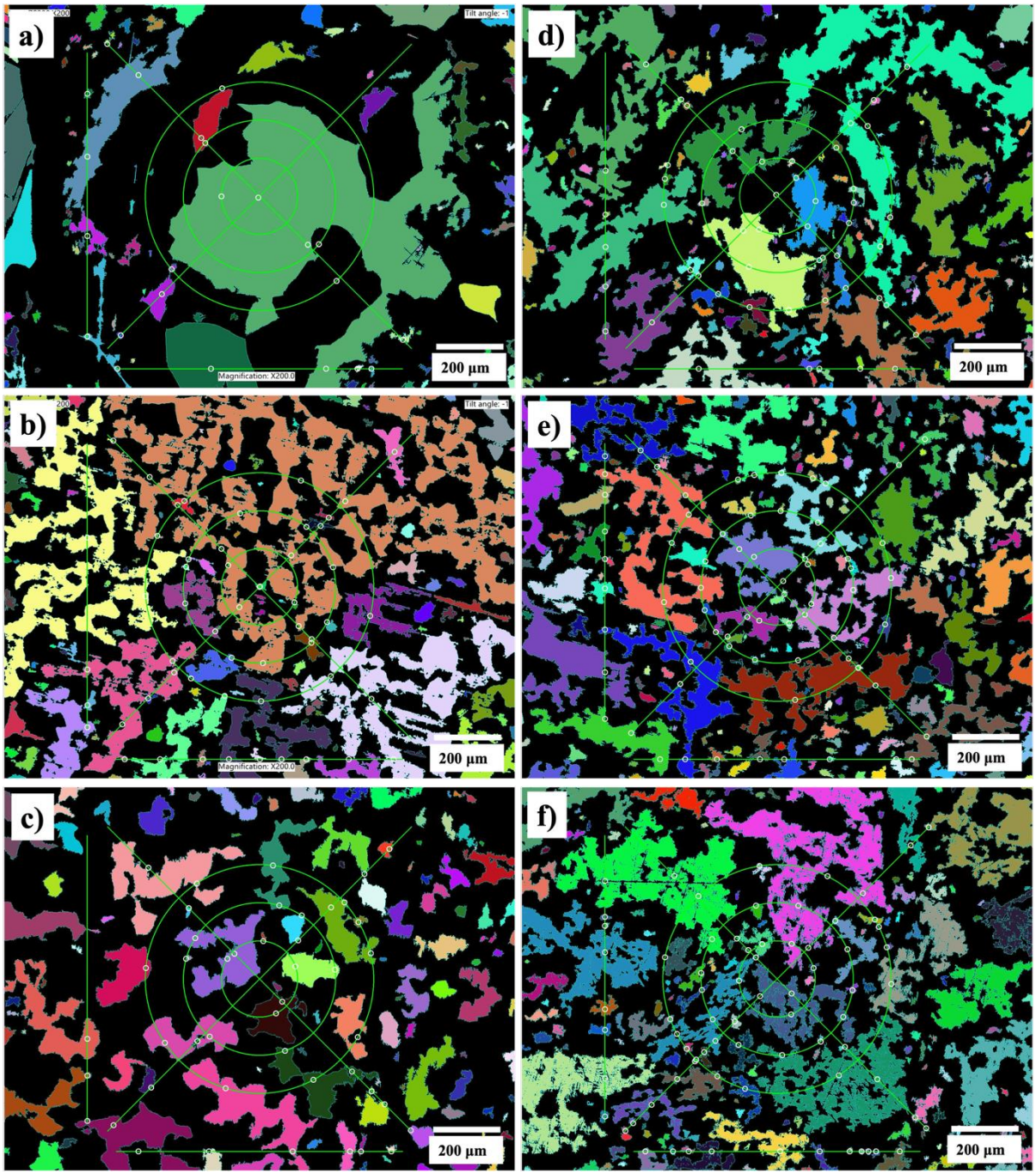

Figure 3: Grain segmentation maps correspond to the micrographs in Figure 2 (a-f), illustrating changes in grain size, boundary density, and recrystallisation extent across heat-treatment durations. Measurement grids overlay each segmentation map to support grain-size quantification.

After homogenisation at 390 °C, the dendritic outlines remain visible (green arrows in Figure 2(b)), but the contrast between dendrite cores and interdendritic regions decreases a sign of Mn diffusion into the surrounding Zn matrix. The segmentation map in Figure 3(b) shows elongated, partially restored grain boundaries, yet the grain morphology still reflects the inherited cast structure. This stage reduces chemical heterogeneity but does not yet refine grain morphology significantly, setting the stage for recrystallisation during subsequent annealing. Similar observations have been reported by Pilchak et al. [23] during beta annealing of Ti-6Al-4V, where homogenisation primarily serves to reduce solute gradients before recrystallisation begins.

Annealing at 400 °C for 1 h initiates clear dissolution of dendritic features (orange arrows in Figure 2(c)). The original cast boundaries begin to break down, and smaller recrystallised grains emerged along former interdendritic interfaces. In Figure 3(c), numerous small grains appear alongside remnants of the original large grains, confirming that this stage corresponds to partial recrystallisation coupled with recovery processes. This transitional structure is critical, reducing dislocation density and smoothing compositional gradients. Yang et al. [24] observed a similar phenomenon in cold-rolled Cu-Ni-P alloys, where partial recrystallisation preferentially nucleated at grain boundaries and twin interfaces. The present Zn-2.4Mn exhibits analogous behaviour, though the HCP structure of Zn leads to more heterogeneous nucleation compared to the FCC Cu alloy due to limited slip systems [25].

At 2 h, dendritic remnants are essentially absent (Figure 2(d)). The microstructure displays a more uniform distribution of grains, and boundaries are sharper and more continuous. The segmentation map (Figure 3(d)) shows extensive grain fragmentation and formation of equiaxed grains, indicating that recrystallisation is now well advanced. Mn, previously concentrated within interdendritic regions, is more evenly redistributed, resulting in a more stable recrystallised matrix. This refinement stage corresponds to the expected improvement in mechanical properties such as strength and hardness. Jang et al. [26] reported that in low-carbon TRIP steel, 2 h annealing at optimal temperature produces the maximum recrystallised fraction before grain growth initiates. The present Zn-2.4Mn follows a comparable kinetic pathway, although the cast Zn alloy requires longer annealing (2-3 h) to achieve full recrystallisation compared to the cold-worked TRIP steel (~1 h), reflecting differences in stored energy and crystal structure.

After 3 h of annealing, the microstructure reaches its most refined and uniform state. Figure 2(e) shows complete elimination of the cast dendritic morphology, replaced by fine equiaxed grains throughout the field of view. Figure 3(e) confirms this microstructure with the highest grain-boundary density and most homogeneous grain-size distribution across all conditions. This condition represents full recrystallisation without overgrowth, a configuration typically associated with maximum hardness and yield strength due to the Hall–Petch effect. The refined grain structure also supports more uniform plastic deformation. As reviewed by Naik and Walley [27], the Hall-Petch relationship ($\sigma = \sigma_0 + kd^{-1/2}$) accurately describes grain-size strengthening in the micrometer regime, which applies to the present grain sizes (>45 μm equivalent diameter). Unlike the nanocrystalline materials discussed in [26], the present alloy shows no evidence of inverse Hall-Petch behaviour, as grain sizes remain well above the 30 nm threshold where such transitions occur.

At 4 h, grain coarsening becomes evident. While the recrystallised equiaxed morphology persists (Figure 2(f)), selected grains begin to grow larger at the expense of neighbouring grains. The segmentation map (Figure 3(f)) highlights this early-stage grain-growth behaviour through a wider spread in grain sizes. This structural coarsening reduces total grain-boundary area, which typically lowers hardness and strength but enhances ductility. Ueki et al. [28] demonstrated that over-annealing in Co-Cr-W-Ni alloys leads to strength reduction, though ductility initially increases before declining due to strain localization. In the present Zn-2.4Mn, the 4 h condition shows simultaneous loss of both strength and ductility, suggesting that the HCP structure of Zn promotes earlier strain localization upon grain coarsening compared to the fcc Co-based alloy studied in [27]. The contrast between Figures 3(e) and 3(f) illustrates the sensitivity of Zn–Mn microstructure to annealing duration, emphasizing that 3 h represents the optimal balance between refinement and stability.

3.2 Quantitative Microstructure–Property Correlation

The qualitative microstructural evolution described in Figures 2 and 3 is quantitatively substantiated by the data in Table 1. This data reveals a definitive and non-linear relationship between annealing duration, grain refinement, and the resulting mechanical properties of the Zn-2.4Mn alloy. The measured average grain area provides a critical numerical counterpart to the optical micrographs. The as-cast condition, with its coarse dendritic arms, shows a large average grain size (5416.55 μm²). The subsequent increase in calculated grain area after homogenization (6834.19 μm²) is an artifact of the measurement method transitioning from delineating fine dendritic networks to identifying larger, more continuous grains as interdendritic boundaries dissolve. This aligns with the observed fading of dendritic contrast (Figure 2(b)). The true refinement process begins with annealing. A consistent reduction in grain area is observed from the 1-hour (4684.46 μm²) to the 3-hour anneal (3263.32 μm²), directly correlating with the microstructural progression from partial to complete recrystallisation (Figures 2(c–e)). This refinement follows the Hall-Petch principle, where an increasing density of grain boundaries strengthens the material by impeding dislocation motion. The reversal of this trend at 4 hours (4168.23 μm²) provides quantitative confirmation of the grain coarsening visually identified in Figure 2(f), marking the transition from a refined to an over-aged microstructure.

Table 1: Effect of heat-treatment duration on the microstructure and mechanical properties of Zn–2.4Mn alloy: (a) as-cast, (b) homogenised, (c) 1 h, (d) 2 h, (e) 3 h, (f) 4 h, showing corresponding values for average grain size (μm), Vickers hardness (HV), UTS (MPa), and elongation (%). The table highlights the evolution of microstructure and mechanical response as a function of heat-treatment duration

Sample	Average Grain Size (μm²)	Hardness (HV)	UTS (MPa)	Strain (%)
As Cast	5416.55	53.12 ± 6.31	28.33 ± 10.53	2.84 ± 0.70
Homogenised	6834.19	55.39 ± 3.44	102.06 ± 31.19	6.10 ± 4.01
Anneal 1 h	4684.46	56.40 ± 4.93	103.38 ± 20.14	4.38 ± 0.87
Anneal 2 h	4072.81	67.97 ± 6.46	116.15 ± 13.79	4.54 ± 0.92
Anneal 3 h	3263.32	73.13 ± 4.92	152.92 ± 21.58	7.31 ± 1.42
Anneal 4 h	4168.23	74.73 ± 4.47	113.25 ± 18.68	4.59 ± 1.06

The Hall-Petch strengthening observed in this study is consistent with recent findings on Zn-Mn alloys. Chan et al. [11] reported that increasing Mn content up to 2.4 wt.% progressively refines grain size from 626 μm to 282 μm, with grain boundary strengthening identified as the dominant mechanism. Similarly, Zhu et al. [29] demonstrated that Mn additions up to 0.5 wt.% activate both solid solution and precipitation strengthening via $MnZn_{13}$ formation. A quantitative comparison with [27] reveals that the present Zn-2.4Mn achieves higher UTS (152.92 MPa) than Zn-0.5Mn (~120 MPa), confirming that higher Mn content further enhances strength via increased volume fraction of $MnZn_{13}$. However, ductility in the present alloy (7.31 % at 3 h) is lower than Zhu's Zn-0.5Mn (~15 %), indicating a clear strength-ductility trade-off at high Mn levels that was not observed at lower Mn concentrations [28]. The present results extend Chan et al. [11] findings by systematically tracking microstructure and property evolution as a function of heat-treatment duration at a fixed 2.4 wt.% Mn composition.

The mechanical properties exhibit a complex dependence on the microstructural state. Hardness (HV) shows a monotonic increase from the as-cast state (53.12 HV) to the 4-hour anneal (74.73 HV). The initial, modest rise after homogenization and 1-hour annealing (to ~56 HV) corresponds to recovery and the reduction of chemical gradients. The significant jump to 67.97 HV at 2 hours coincides with advanced recrystallisation and a more equiaxed grain structure. The maximum hardness of 73.13 HV at the point of peak refinement (3 hours) is a clear manifestation of Hall-Petch strengthening [24]. The continued slight increase in hardness at 4 hours (74.73 HV), despite grain coarsening, suggests

supplementary strengthening mechanisms such as possible fine-scale precipitation or solid-solution stabilization may become active during prolonged annealing, decoupling hardness from grain size at this stage.

The ultimate tensile strength (UTS) presents a more pronounced optimum linked directly to grain size. The as-cast alloy exhibits poor strength (28.33 MPa) and ductility (2.84 %), characteristic of a brittle, segregated dendritic network. Homogenization drastically improves UTS (102.06 MPa) and strain to failure (6.10 %) by mitigating micro-segregation. While the 1- and 2-hour anneals maintain UTS levels around 103-116 MPa, the 3-hour anneal yields the superior tensile performance, with UTS peaking at 152.92 MPa. This peak strength is achieved concurrently with the finest grain structure and the highest ductility (7.31 %) among all processed conditions, demonstrating an exceptional balance of properties.

This balance is disrupted by over-annealing. The 4-hour sample shows a marked decrease in UTS to 113.25 MPa and a reduction in ductility to 4.59 %, directly attributable to the onset of grain coarsening. The reduction in grain boundary area diminishes the Hall-Petch strengthening effect, lowering strength. The associated drop in ductility may result from less homogeneous strain distribution and potential strain localization within the coarsening grain structure [29]. The data illustrates a key processing challenge: maximizing both strength and ductility simultaneously. The 3-hour anneal successfully achieves this, as the refined, uniform grain structure facilitates widespread dislocation activity and grain boundary sliding, enhancing ductility, while the high grain boundary density concurrently elevates strength. In contrast, the as-cast and coarsened (4-hour) conditions exhibit poorer combinations, highlighting that an intermediate, fully recrystallised state is essential for optimal comprehensive mechanical performance in this alloy system. Our previous work [11] reported that annealing Zn-2.4Mn at 400 °C for up to 3 h reduces dislocation density by approximately 23 % and refines grain size from 263 µm to 45 µm. The present results are in excellent quantitative agreement with [30], while extending the analysis to directly link refinement to tensile properties (UTS and elongation), providing a more complete processing–microstructure–property correlation.

3.3 Indentation Topology and Cross-Section Strain Analysis

Figure 4 presents the 3D indentation topology for each heat-treatment condition, while Figure 5 provides the cross-section indentation analysis from which the elongation (strain %) values reported in Table 1 were derived. The numerical height values extracted from the scans, combined with cross-sectional strain measurements, provide critical insight into how microstructural evolution governs localized deformation and overall tensile ductility.

In the as-cast condition (Figure 4(a) and 5(a)), the maximum height variation around the indent (~57.59 µm) reflects the large, unconstrained plastic zone typical of coarse dendritic grains. The cross-section analysis (Figure 5(a)) reveals an irregular deformation profile with non-uniform strain distribution, corresponding to the low elongation value (2.84 % ± 0.70 %). This poor ductility is characteristic of the brittle, segregated dendritic network where crack initiation occurs preferentially along interdendritic boundaries.

After homogenisation (Figure 4(b) and 5(b)), the pile-up height decreases slightly to ~53.86 µm. Although the microstructure remains coarse, the reduction in chemical segregation improves deformation uniformity, producing a more symmetric topography. The cross-section analysis (Figure 5(b)) shows a more regular indentation profile, correlating with improved elongation (6.10 % ± 4.01 %). This significant increase in ductility demonstrates that homogenisation effectively reduces strain localization by mitigating micro-segregation, consistent with the observations of Jang et al. [26] regarding homogenisation-induced improvements in deformation uniformity.

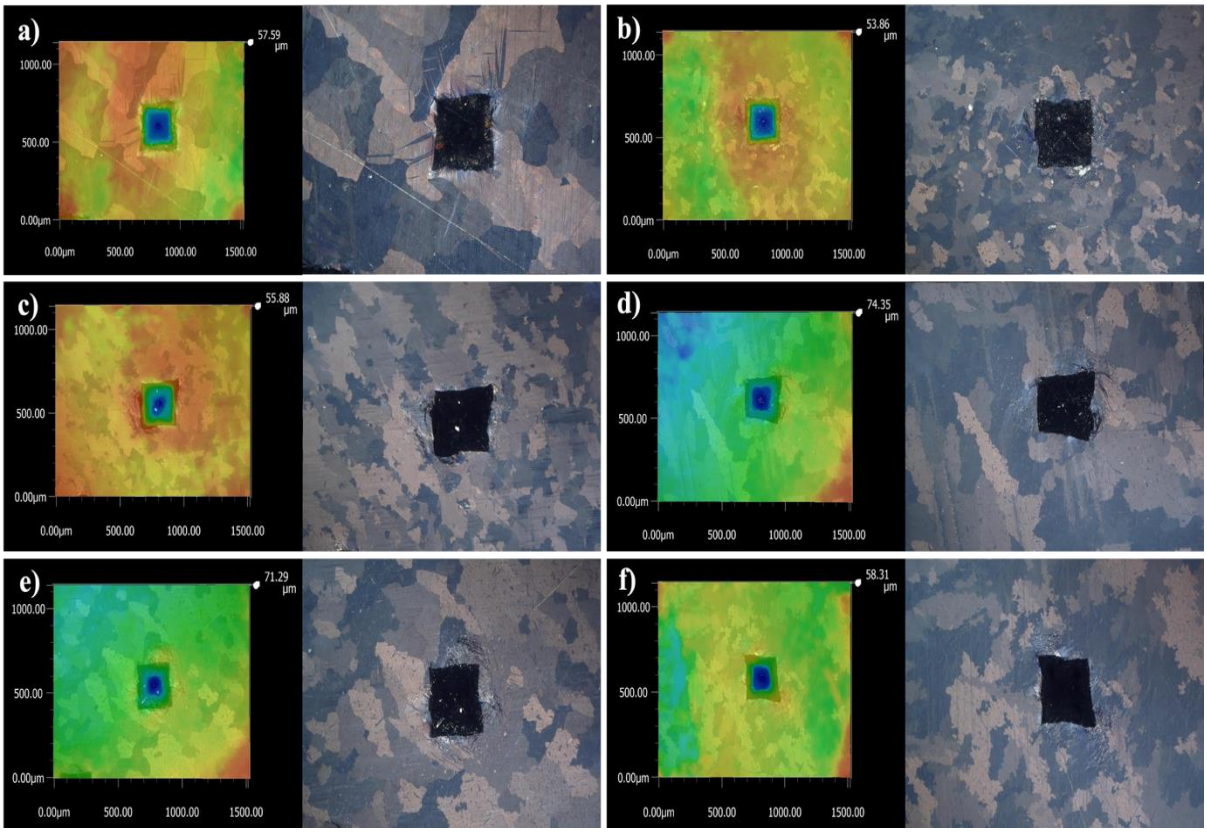

Figure 4: Optical microscopy images showing the surface morphology and indentation topology of the Zn–Mn alloy under different processing conditions: (a) as-cast, (b) homogenised, (c) annealed for 1 h, (d) annealed for 2 h, (e) annealed for 3 h, and (f) annealed for 4 h. The images illustrate the evolution of surface features and deformation response with heat treatment

At 1 h annealing (Figure 4(c) and 5(c)), the indent height (~55.88 µm) remains comparable to previous conditions, but the pile-up becomes more uniform. The cross-section analysis (Figure 5(c)) reveals a deformation profile with moderate symmetry, corresponding to an elongation of 4.38 % ± 0.87 %. The slight decrease in ductility compared to the homogenised condition suggests that early recrystallisation stages may temporarily reduce strain accommodation before full recrystallisation is achieved. Yang et al. [24] observed a similar temporary ductility dip during partial recrystallisation in Cu-Ni-P alloys, attributed to the coexistence of recovered and unrecrystallised regions creating strain incompatibility.

A notable change occurs at 2 h annealing (Figure 4(d) and 5(d)), where the maximum topographical height increases sharply to ~74.35 µm. This counterintuitive rise coincides with substantial recrystallisation: the fine, equiaxed grains developed at this stage promote more uniform but deeper indentation penetration before work-hardening mechanisms activate. The cross-section analysis (Figure 5(d)) shows a well-developed, symmetric deformation zone, corresponding to an elongation of 4.54 % ± 0.92 %. While ductility remains moderate, the significant increase in hardness (67.97 HV) and UTS (116.15 MPa) at this stage indicates that recrystallisation is now well advanced. At this Mn content (2.4 wt.%), the Zn-Mn system lies well within the precipitation-dominated regime described by Zhu et al. [29], where $MnZn_{13}$ particles provide additional strengthening. The 2 h annealing condition represents a state where these particles are partially dissolved, reducing pinning effects and allowing recrystallisation to progress [28].

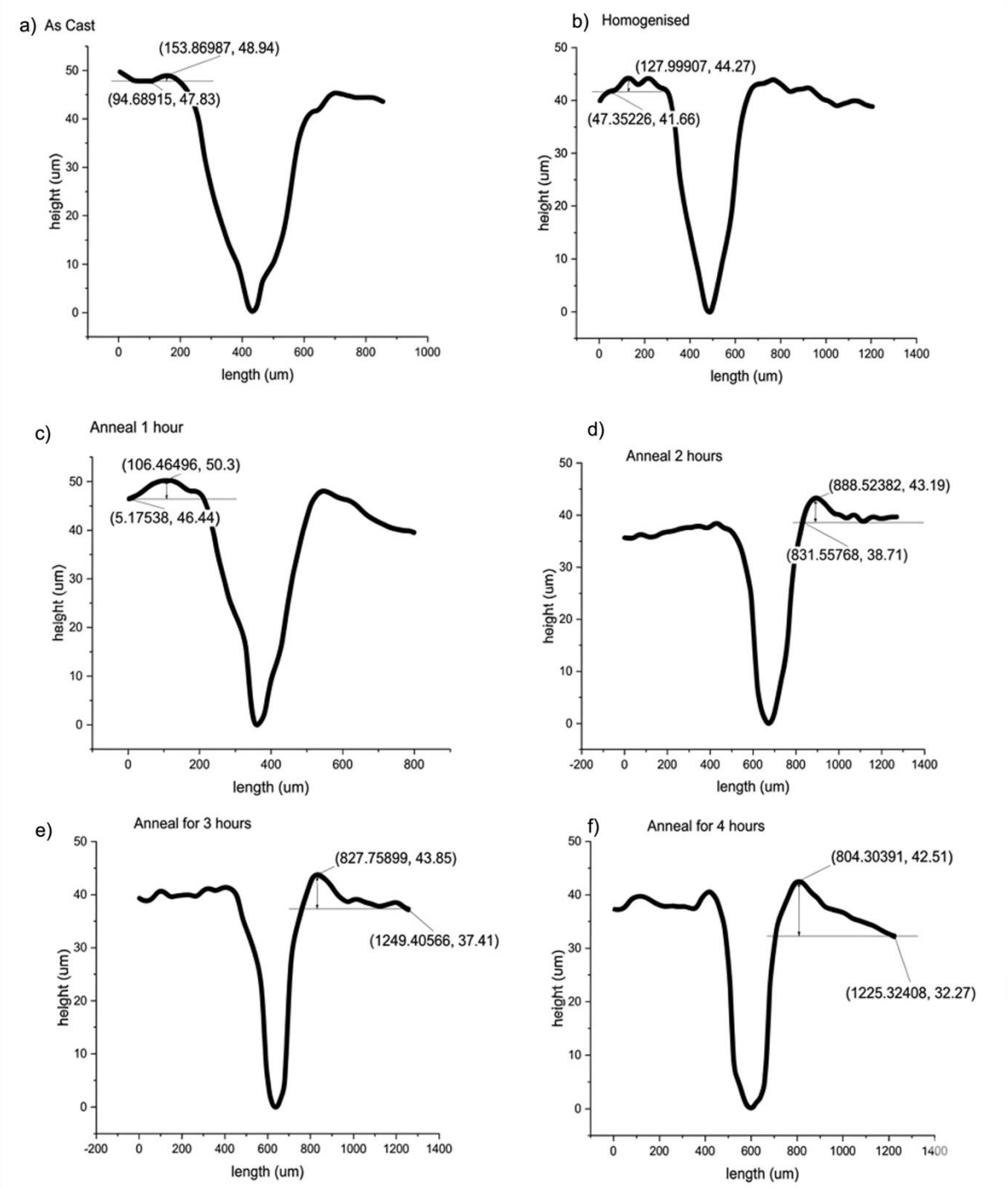

Figure 5: Cross-section indentation analysis of the Zn–Mn alloy under different processing conditions: (a) as-cast, (b) homogenised, (c) annealed for 1 h, (d) annealed for 2 h, (e) annealed for 3 h, and (f) annealed for 4 h. This analysis provided the deformation details of the indented point for each samples, respectively.

The 3 h annealed condition (Figure 4(e) and 5(e)) shows a slightly reduced height (~71.29 μm) compared to the 2 h sample, consistent with the transition into a fully recrystallised microstructure. The refined grains (3263 μm²) provide more grain-boundary resistance, limiting lateral plastic flow and stabilizing the deformation zone. The cross-section analysis (Figure 5(e)) reveals the most uniform and

symmetric deformation profile among all conditions, corresponding to the peak elongation of 7.31 % ± 1.42 %. This maximum ductility coincides with peak UTS (152.92 MPa) and near-peak hardness (73.13 HV), demonstrating that the 3 h condition achieves an exceptional balance of strength and ductility. As reviewed by Naik and Walley [27], Hall-Petch strengthening produces peak strength at the finest grain size, while our previous work [30] confirmed that 3 h annealing reduces dislocation density by 23 %. The present results integrate these findings: the fully recrystallised structure (low dislocation density) combined with fine grain size (Hall-Petch strengthening) simultaneously enhances both strength and ductility a combination not always achievable in metallic alloys.

Finally, after 4 h annealing (Figure 4(f) and 5(f)), the indentation height decreases to ~58.31 µm, returning to values similar to the as-cast condition. This reduction reflects grain coarsening: larger grains reduce boundary density, allowing plastic deformation to relax more broadly and lowering the maximum displacement. The cross-section analysis (Figure 5(f)) shows a less uniform deformation profile compared to the 3 h condition, with evidence of strain localization. Correspondingly, elongation decreases to 4.59 % ± 1.06 %, and UTS drops to 113.25 MPa. Ueki et al. [28] demonstrated that over-annealing beyond the optimal recrystallisation window leads to strain localization and reduced ductility. The present Zn-2.4Mn follows this pattern, with the 4 h condition showing simultaneous loss of strength and ductility a characteristic of over-aged microstructures where grain coarsening promotes heterogeneous deformation [26].

The present results align with our previous study on as-cast Zn-Mn alloys [11], which established that 2.4 wt.% Mn produces optimal grain refinement (282 ± 7 µm) and hardness (51.2 HV) via solid solution and $MnZn_{13}$ precipitation. Upon annealing at 400 °C, the observed evolution in grain size, hardness, UTS, and elongation follows the expected Hall-Petch strengthening trend, consistent with Chan et al. [31], who reported that annealing up to 3 h reduces dislocation density and refines grain size from 263 µm to 45 µm in Zn-2.4Mn. The trade-off between strength (peak at 2-3 h) and ductility (peak at 3 h) observed here mirrors the behaviour reported by Zhu et al. [29] for Zn-Mn alloys transitioning from solid solution to precipitation-dominated strengthening. Collectively, these comparisons confirm that the present findings are scientifically grounded in established Zn-Mn metallurgy.

4. CONCLUSIONS

Heat treatment of the Zn-2.4Mn alloy established a clear processing-microstructure-property relationship. Grain size decreased from 5416.55 µm² (as-cast) to a minimum of 3263.32 µm² after 3 h annealing, confirming complete recrystallization before coarsening at 4 h (4168.23 µm²). Hardness increased steadily from 53.12 HV to 73.13 HV at 3 h, while UTS and elongation peaked at the same condition (152.92 MPa, 7.31 % strain). Indentation topology showed the most stable deformation response in the 3 h sample. This work is the first to systematically map the annealing duration property relationship for Zn-2.4Mn, identifying 400 °C for 3 h as the optimal heat-treatment condition. The findings establish a benchmark for microstructure–property optimization in high-Mn Zn alloys, offering a foundation for future alloy design requiring tailored mechanical performance.

Acknowledgements

This work was supported by the Universiti Teknologi Malaysia through F4 Hi-Tech research grant (Q.J130000.4624.00Q08) and the Professional Development Research University grant (Q.J130000.21A2.07E37). This support was essential for the successful completion of this research.

Author Contributions

All authors contributed toward data analysis, drafting and critically revising the paper and agree to be accountable for all aspects of the work.

Disclosure of Conflict of Interest

The authors have no disclosures to declare.

Compliance with Ethical Standards

The work is compliant with ethical standards.

References

[1] Yang, H., Zhu, D., Li, G., Jia, B., Qu, X., Zheng, Y., Lin, W., Dai, K. & Zhang, Z. (2020). Alloying design of biodegradable zinc as promising bone implants for load-bearing applications. *Nature Communications*, 11(1), 401.

[2] Michalak, M., Łatka, L., Sokołowski, P., Candidato, R. T. & Ambroziak, A. (2021). Effect of TiO_2 on the microstructure and phase composition of Al_2O_3 and Al_2O_3–TiO_2 APS sprayed coatings. *Bulletin of the Polish Academy of Sciences: Technical Sciences*, 69(2), e136735.

[3] Hussain, M., Ullah, S., Raza, M. R., Abbas, N. & Ali, A. (2022). Recent developments in Zn-based biodegradable materials for biomedical applications. *Journal of Functional Biomaterials*, 14(1), 1.

[4] Boukalová, A., Kubásek, J., Nečas, D., Minárik, P., Donik, Č., Dvorský, D., Vojtěch, D., Michalcová, A., Godec, M. & Paulin, I. (2024). Harmonizing microstructures and enhancing mechanical resilience: Novel powder metallurgy approach for Zn–Mg alloys. *Journal of Materials Research and Technology*, 31, 2807–2819.

[5] Kong, L., Heydari, Z., Lami, G. H., Saberi, A., Baltatu, M. S. & Vizureanu, P. (2023). A Comprehensive Review of the Current Research Status of Biodegradable Zinc Alloys and Composites for Biomedical Applications. *Materials*, 16(13), 4797.

[6] Wei, L. & Gao, Z. (2023). Recent research advances on corrosion mechanism and protection, and novel coating materials of magnesium alloys: a review. *RSC Advances*, 13(12), 8427–8463.

[7] Hassan, S. F., Islam, M. T., Saheb, N. & Baig, M. M. A. (2022). Magnesium for Implants: A Review on the Effect of Alloying Elements on Biocompatibility and Properties. *Materials*, 15(16), 5669.

[8] Ramalingam, V. V., Ramasamy, P., Kovukkal, M. D. & Myilsamy, G. (2019). Research and development in magnesium alloys for industrial and biomedical applications: a review. *Metals and Materials International*, 26(4), 409–430.

[9] Nečas, D., Marek, I., Pinc, J., Vojtěch, D. & Kubásek, J. (2022). advanced zinc–magnesium alloys prepared by mechanical alloying and spark plasma sintering. *Materials*, 15(15), 5272.

[10] Cipriano, A. F., Johnson, I., Zhao, T., Liu, H., Garcia, S. & Guan, R.-G. (2013). In vitro degradation of four magnesium–zinc–strontium alloys and their cytocompatibility with human embryonic stem cells. *Journal of Materials Science: Materials in Medicine*, 24(4), 989–1003.

[11] Chan, K. F., Supee, A., Tanemura, M., Hidetoshi, M. & Mohd Yusop, M. Z. (2025). Microstructural refinement and intermetallic strengthening in Zn–Mn alloys. *Journal of Materials Science*. 61(2), 1297-1308.

[12] Chan, K. F., Tanemura, M., Yaakob, Y. & Yusop, M. Z. M. (2025). Influence of Mn content on microhardness in Zn-Mn/CNF cubical cast alloys: A 3D topographical study. *Journal of Alloys and Compounds*, 1012, 178486.

[13] Oliver, A. A., Kolesar, T. M., Morath, L. M., Guillory, R. J., Drelich, J. W., Goldman, J., Flom, K. L., Mostaed, E. & Sikora-Jasinska, M. (2020). Analysis of vascular inflammation against bioresorbable Zn-Ag based alloys. *ACS Applied Bio Materials*, 3(10), 6779–6789.

[14] Antoniac, I., Miculescu, F., Cotrut, C., Ficai, A., Rau, J. V., Grosu, E., Antoniac, A., Tecu, C. & Cristescu, I. (2020). Controlling the degradation rate of biodegradable Mg–Zn-Mn alloys for orthopedic applications by electrophoretic deposition of hydroxyapatite coating. *Materials*, 13(2), 263.

[15] Ren, T., Song, Z., Liu, H., Sun, W., Yang, L., Chen, Y., Xu, C., Guo, P. & Gao, X. (2019). Evaluation of as-extruded ternary Zn–Mg–Zr alloys for biomedical implantation material: In vitro and in vivo behavior. *Materials and Corrosion*, 70(6), 1056–1070.

[16] Zhao, L., Zhuo, X., Gao, W., Zhao, S., Liu, H., Hu, Z., Zhang, P., Wu, Y., Jiang, J. & Ma, A. (2023). A bimodal grain structured Zn–0.5Ag–0.2Mg alloy with high strength and ductility achieved through combined ECAP and cold rolling. *Journal of Materials Research and Technology*, 24, 3222–3234.

[17] Tong, X., Miao, D., Zhou, R., Shen, X., Luo, P., Ma, J., Li, Y., Lin, J., Wen, C. & Sun, X. (2024). Mechanical properties, corrosion behavior, and in vitro and in vivo biocompatibility of hot-extruded Zn-5RE (RE = Y, Ho, and Er) alloys for biodegradable bone-fixation applications. *Acta Biomaterialia*, 185, 55-72.

[18] Westhauser, F., Rehder, F., Peukert, W., Nawaz, Q., Hohenbild, F., Moghaddam, A., Boccaccini, A. R., Ali, M. S., Fellenberg, J., Wilkesmann, S. & Saur, M. (2020). Effect of manganese, zinc, and copper on the biological and osteogenic properties of mesoporous bioactive glass nanoparticles. *Journal of Biomedical Materials Research Part A*, 109(8), 1457–1467.

[19] Dong, C., Liao, Z., Yin, Y., Yi, Y., Zhu, G., Zheng, T., Tan, Q. & Xie, Y. (2025). Effects of Nanoscale precipitates on mechanical properties, corrosion resistance, and biocompatibility in Zn-Mn alloy. *Scientific Reports*, 15(1), 5454.

[20] Cheng, X., Lin, Q., Jin, H., Han, F., Dou, X., Zhang, X., He, Z., He, C., Zhao, S. & Zhang, D. (2025). Effect of Mn content on the corrosion behavior and biocompatibility of biodegradable Zn-Mn alloys. *Scientific Reports*, 15, 8958.

[21] Zuiko, I. S., Kaibyshev, R. O. & Gazizov, M. R. (2016). Effect of thermomechanical treatment on the microstructure, phase composition, and mechanical properties of Al–Cu–Mn–Mg–Zr alloy. *The Physics of Metals and Metallography*, 117(9), 906–919.

[22] Amer, S., Barkov, R., Prosviryakov, A., Pozdniakov, A., Yakovtseva, O., Medvedeva, S., Bazlov, A. & Loginova, I. (2020). the phase composition and mechanical properties of the novel precipitation-strengthening Al-Cu-Er-Mn-Zr alloy. *Applied Sciences*, 10(15), 5345.

[23] Pilchak, A. L., Semiatin, S. L. & Sargent, G. A. (2017). Early Stages of microstructure and texture evolution during beta annealing of Ti-6Al-4V. *Metallurgical and Materials Transactions A*, 49(9), 908–919.

[24] Yang, W., He, J., Zhang, C., Zhang, N., Zhang, C. & Gao, W. (2024). Microstructure and texture evolution of Cu-Ni-P alloy after cold rolling and annealing. *Materials*, 17(11), 2696.

[25] Gerald Edmunds. (1944). Miscellaneous Alloys - Liquidus Determinations in Zinc-rich Alloys (Zn-Fe; Zn-Cu; Zn-Mn). The American Institute of Mining, Metallurgical, and Petroleum Engineers.

[26] Jang, J-M., Cho, K-M., Suh, D-W., Kim, S-J. & Kang, N. H. (2009). Effects of annealing conditions on microstructure and mechanical properties of low carbon, manganese transformation-induced plasticity steel. *Metals and Materials International*, 15(6), 909–916.

[27] Naik, S. N. & Walley, S. M. (2019). The Hall-Petch and inverse Hall-Petch relations and the hardness of nanocrystalline metals. *Journal of Materials Science*, 55, 2661–2681.

[28] Ueki, K., Yanagihara, S., Ueda, K., Nakai, M., Nakano, T. & Narushima, T. (2019). Overcoming the strength-ductility trade-off by the combination of static recrystallization and low-temperature heat-treatment in Co-Cr-W-Ni alloy for stent application. *Materials Science and Engineering: A*, 766, 138400.

[29] Zhu, X., Ren, T., Guo, P., Yang, L., Shi, Y., Sun, W. & Song, Z. (2022). Strengthening mechanism and biocompatibility of degradable Zn-Mn alloy with different Mn content. *Materials Today Communications*, 31(10), 103639.

[30] Guan, D., Rainforth, W. M., Gao, J., Ma, L. & Wynne, B. (2017). Individual effect of recrystallisation nucleation sites on texture weakening in a magnesium alloy: Part 2- shear bands. *Acta Materialia*, 145, 399–412.

[31] Chan, K. F., Ng, C. L., Nazrim, B. B. H., Yaakob, Y., Miyazaki, H., Tanemura, M. & Yusop, M. Z. M. (2026). Role of annealing duration on grain distribution and fracture mechanisms in Zn–Mn alloy. *Journal of Alloys and Compounds*, 1058, 186962.